This is the peer reviewd version of the followng article:

Surface Immobilized His-tagged Azurin as a Model Interface for the Investigation of Vectorial Electron Transfer in Biological Systems / Casalini, Stefano; Berto, Marcello; Kovtun, Alessandro; Operamolla, Alessandra; DI ROCCO, Giulia; Facci, Paolo; Liscio, Andrea; Farinola, Gianluca M.; Borsari, Marco; Bortolotti, Carlo Augusto. - In: ELECTROCHIMICA ACTA. - ISSN 0013-4686. - 178:(2015), pp. 638-646. [10.1016/j.electacta.2015.07.156]

Terms of use:

The terms and conditions for the reuse of this version of the manuscript are specified in the publishing policy. For all terms of use and more information see the publisher's website.

19/04/2024 21:31

(Article begins on next page)

Surface Immobilized His-tagged Azurin as a Model Interface for the Investigation of Vectorial Electron Transfer in Biological Systems.

Stefano Casalini[a], Marcello Berto[a], Alessandro Kovtun[b,c], Alessandra Operamolla[d], Giulia Di Rocco[a], Paolo Facci[f], Andrea Liscio[b], Gianluca M.Farinola[d], Marco Borsari[e], Carlo A. Bortolotti[a,g,*]

[a]*Department of Life Sciences, University of Modena and Reggio Emilia, Via G. Campi 103, 41125, Modena (Italy)*
[b]*Istituto per la Sintesi Organica e la Fotoreattivitá-Consiglio Nazionale delle Ricerche (ISOF-CNR), via Gobetti 101, 40129 Bologna (Italy)*
[c]*Department of Physical, Informatic and Mathematical Sciences, University of Modena and Reggio Emilia, Via G. Campi 213/a, 41125 Modena (Italy)*
[d]*Department of Chemistry, University of Bari, Via E. Orabona 4, 70125 Bari (Italy)*
[e]*Department of Chemical and Geological Sciences, University of Modena and Reggio Emilia, Via G. Campi 103, 41125, Modena (Italy)*
[f]*CNR - Institute of Biophysics, Via De Marini, 6 - 16149 Genova (Italy)*
[g]*Centro S3 - CNR-NANO Istituto Nanoscienze-CNR, Via Campi 213/a, 41125 Modena (Italy)*

Abstract

A model system for the electrochemical investigation of vectorial electron transfer in biological systems was designed, assembled and characterized. Gold electrodes, functionalized with a -OCH_3 terminated, aromatic self-assembled monolayer, were used as a substrate for the adsorption of variants of copper-containing, redox metalloprotein azurin. The engineered azurin bears a polyhistidine tag at its C-terminus. Thanks to the presence of the solvent exposed tag, which chelates Cu^{2+} ions in solution, we introduced an exogenous redox centre. The different reduction potentials of the two redox centres and their positioning with respect to the surface are such that electron transfer from the exogenous copper centre and the electrode is mediated by the native azurin active site, closely paralleling electron transfer processes in naturally occurring multicentre metalloproteins.

*Corresponding author
Email address: carloaugusto.bortolotti@unimore.it (Carlo A. Bortolotti)

Keywords: Vectorial electron transfer, SAM, Azurin, intramolecular rate constant, His-tag

1. Introduction

Electron transfer (ET) reactions are essential steps of the energy transduction pathways in living systems [1]. In particular, vectorial ET, *i.e.* the unidirectional, intra- or intermolecular flow of electrons occurring between different redox centres [2], constitutes the basis for respiratory and photosynthetic processes. In living organisms, biological vectorial ET may be either intramolecular, *i.e.* between multiple redox centres located within the same macromolecule (a typical example is provided by multi-heme proteins), or take place between two distinct biological partners that transiently form a complex, to facilitate the intermolecular flow of electrons.

The former kind has gained increasing attention in the last few years, with the twofold aim of elucidating the mechanisms underlying these fascinating molecular machineries [3, 4, 5, 6] and be inspired by systems such as multiheme proteins to design molecular wires for nanobiotechnological applications [7, 8, 9, 10].

Diheme cytochromes are one of the simplest multicentre metalloproteins: electrochemical investigations of surface immobilized proteins featuring two heme centres have paved the way for the elucidation of how structural and dynamic features affect the relationship between interfacial and intramolecular ET processes [11, 12, 13]. Although the number of multiredox metalloproteins that is being investigated is constantly increasing [14, 15, 16], the possibility of possessing a simple, flexible model system, would certainly be a huge step forward towards the elucidation of the molecular determinants to vectorial ET: ideally, such a system should be easily engineerable and produced as a recombinant species in high yield, and feature two spatially separated metal centres, with sufficiently different reduction potential ($E^{0'}$), to detect their redox process as distinct electrochemical signals.

Engineering a protein by introducing a polyhistidine-tag (His-tag hereafter) at its N- or C-terminus has proved to be a tremendously efficient and time-saving strategy for the purification of recombinant species [17]. The His-tag, typically composed by six units, is usually removed after the purification steps by enzymatic digestion. Nevertheless, its high affinity for metal cations can be conveniently exploited in the pursuit of technological goals, such as the controlled binding of a biomolecule at a metal electrode, either bare (e.g. nickel [18, 19] or gold [20, 21]) or functionalized with a self-assembled-monolayer (SAM),whose terminal group can chelate bivalent metal ions such as Ni^{2+}[22].

Here, we exploited the presence of a terminal His-tag to implement an engineered metalloprotein (azurin) that features two separate copper-based, redox active sites, which could serve as a flexible model system for the investigation of fundamental aspects of vectorial ET. Azurin from *P. aeruginosa* has been extensively employed as a paradigmatic system for the study of biological electron transfer [23, 1, 24, 25, 26, 27, 28, 29]. We used an azurin variant, which possesses a six-residues-long His-tag at its C-terminal end (we will address to this species as to "HT-Azu"). The peculiar structure of azurin is particularly suited for our aims: in fact, its native type 1 (T1) site copper (whose coordination shell is composed by two histidines and one cysteine, yielding a trigonal geometry, and two weak axial ligands) is asymmetrically located at one end of the protein, while the C-terminus lies at the opposite side. We planned to exploit the surface exposed His-tag to chelate Cu^{2+} ions, in order to obtain an azurin variant featuring two redox centres, both containing a Cu ion, but characterized by different coordination sets and solvent exposure, and, most notably, separated by the whole length of the azurin structure (approximately 3 nm). This system would, in principle, allow to detect both interfacial ET from the native Cu site to an electrode or to a redox partner, and intramolecular ET from one copper site to the other. Our bioengineered interface relies on a bottom-up approach that takes advantage of an oligoarylene monodentate self-assembled monolayer, which guarantees a robust HT-Az immobilization on polycrystalline gold. The additional copper centre has been then grafted by means of His-tag present on

top this functionalized electrode. We will describe the strategy that was used to introduce the second metal centre, and present its peculiar electrochemical features.

2. Experimental

2.1. Protein expression and purification

HT-Azu from *P. aeruginosa* was expressed and purified as published elsewhere [19]. Oxidised protein solutions were freshly prepared before use in 5 mM Hepes (4-(2-hydroxyethyl)-1-piperazineethanesulfonic acid), pH 7.

2.2. SAM formation, protein adsorption and electrochemical measurements

4-metoxy-terphenyl-4"-methanethiol (MTM) was synthesized following the procedure reported in literature [30, 31]. A 1 mm diameter polycrystalline gold wire was used as a working electrode (WE) in the electrochemical setup; a Pt sheet and a saturated calomel electrode (SCE) served as counter and reference electrode (CE and RE), respectively. The area of the electrode was 16.5 mm^2, and its length was 5 mm. A Vycor (PAR) set ensured the electric contact between the SCE and the working solution. Potentials were calibrated against the MV^{2+}/MV^{+} couple (MV is methylviologen). All the redox potentials reported here are referred to as the standard hydrogen electrode (SHE). The gold WE was cleaned according to previously published procedures [13, 32] and its active area has been estimated by means of the Randles-Sevçik equation. Cyclic voltammetry (CV) experiments were carried out with a Potentiostat/Galvanostat PAR mod. 273 A at different scan rates using a cell for small volume samples (0.5 ml) under an argon atmosphere. The formation of the MTM SAM on previously cleaned polycrystalline gold electrodes was achieved by dipping the electrode in a 0.1 mM MTM solution (dichloromethane as solvent) at room temperature for 20 hours, as previously described [33, 34, 35]. Once the SAM was formed, and after thoroughly rinsing with dichloromethane, followed by methanol and water, the electrode was immersed in a 0.2 mM protein solution in 5 mM Hepes at pH

7 for 5 hrs at 4 °C. The cyclic voltammetry (CV) experiments were then performed by immersing the functionalized electrode in the working solution of the electrochemical cell (typically 10 mM Hepes, 0.1M KCl, pH 7.3, except for the measurements performed at variable scan rates). CVs at increasing scan rates were recorded to determine the ET rate constant at zero driving force, k_s with the Laviron method [36], and were performed at pH 9.2 (see Results and discussion section). Correction for the ohmic drop was performed with the positive feedback method. The exogenous engineered copper centre was introduced by immersion the gold electrode, functionalized with both MTM and HT-Azu, in a 5 mM aqueous solution of $CuSO_4$ for 2 hours, followed by thorough rinsing with water. The experiments were performed at least in duplicate and the formal reduction potentials $E^{0'}$ were found to be reproducible ± 0.005 V. Ultrapure water (MILLIQ) was used throughout. The same three-electrode cell setup was employed to perform Electronic Impedance Spectroscopy (EIS) measurements. EIS was used to measure the Charge Transfer Resistance to the reduction of $[Fe(CN)_6]^{3-/4-}$ (RCT) and capacitance (C) of the SAM.

2.3. KPFM and XPS measurements

Kelvin Probe Force Microscopy (KPFM) measurements were performed in air by employing a commercial microscope Multimode (Bruker) with Extender Electronics module. In order to obtain a sufficiently large and detectable mechanical deflection, we used (k=2.8 Nm^{-1}) Pt/Ir coated ultra-lever silicon tips (SCM, Bruker) with oscillating frequencies in the range between 60-90 KHz. KPFM measurements were obtained using second-pass technique: a topographic line scan is first obtained by Atomic Force Microscopy (AFM) operating in Tapping Mode and then that same line is rescanned in Lift Mode with the tip raised to a lift height of 10 nm. The acquired AFM and KPFM images (not shown in the paper) reveal an uniform morphology and contact potential in the micron scale. For this reason, the values reported in the paper correspond to the average calculated for five images, corresponding to a scanned area of 500 μm^2.

The X-Ray Photoelectron Spectroscopy (XPS) spectra were recorded with

a Phoibos 100 hemispherical energy analyser (Specs) using Mg Kα radiation ($\hbar\omega$ =1253.6 eV). The X-ray power was 250 W. The spectra were recorded in the constant analyser energy (CAE) mode with analyser pass energies of 40 eV for the survey spectra and 20 eV for the high resolution ones. Charging effects were corrected by energy calibration on C 1s level relative to 284.5 eV. The base pressure in the analysis chamber during analysis was 5 x 10^{-10} mbar. All the XPS spectra were performed with an exposure time of about 1 h except the fine spectrum acquired on the sample Au/SAM/HT-Azu having an exposure time of 5 h. All the spectra were normalised to the corresponding acquisition time. During this period no signal alteration was ever detected.

Both KPFM and XPS measurements were performed on golden slides purchased from Phasis (Geneva, Switzerland) with the followng specifications: Au, 50nm thick and 2-3 nm of Ti, as adhesive layer.

3. Results and discussion

3.1. His-tagged-Azurin adsorbed on MTM

The first step of the bottom up approach to the implementation of the bio-(in)organic interface was the formation of the MTM self-assembled monolayer on the gold surface. Evidence of the SAM compactness was provided by EIS measurements, yielding both RCT and C values for the SAM. We could fit the corresponding Nyquist plots by a Randles circuit composed by the solution resistance (RS), a constant phase element (CPE), and the RCT: the fact that the Randles circuit lacks the Warburg component is indeed indicative of the high blocking capability of the SAM (see Figure S1 i the Supporting Information, SI, for the corresponding Nyquist plot). The measured RCT and C values are 895 $\pm$1 kΩcm^{-2} and 218 $\pm$2 nF cm^{-2}, respectively, and are consistent with previously reported values for pinhole-free, oligoarylene thiols-based SAMs on polycrystalline gold [34].

Once the MTM self-assembled monolayer was successfully formed on the gold surface, HT-Azu was immobilized on it. In this context, the azurin adsorp-

tion is likely governed by hydrophobic interaction, as already demonstrated in literature [28, 27]. In particular, the broad hydrophobic region surrounding the metal-binding His117 and Cu ion is most likely responsible for the interaction with the oligoarylene-based SAM. To clear the field from other possible binding patches on hydrophobic SAMs, we mapped the hydrophobic and hydrophilic surface areas of wild-type azurin (PDB code: 4AZU [37]) by using the Platinum WEB server [38], which is based on the empirical concept of Molecular Hydrophobicity Potential (MHP)[39]. The results are displayed in Fig. 1, which shows how the large hydrophobic region (depicted in red), mostly formed by the loop that contains three of the Cu-binding residues and that is known to play a physiological key role [40], is almost the only non-polar, surface exposed area of azurin. A further smaller hydrophobic region is placed on the two C-terminal antiparallel beta sheets. It is therefore reasonable to conclude, as it was previously anticipated [26, 27, 28], that azurin prevalently binds to -OCH_3 terminated SAMs via the hydrophobic patch surrounding its redox active centre.

A typical cyclic voltammogram (CV) for HT-Azu immobilized on MTM SAM formed on polycrystalline gold is shown in Fig. 2. A single electrochemical quasi-reversible process can be observed, originating from the one-electron reduction-oxidation of the protein copper ion. The peak current ratio $i_{cathodic}/i_{anodic}$ is approximately 1 for all the investigated scan rates. The linear dependence of the peak currents as a function of the scan rate indicates that the electrochemical response originates from a redox active species immobilized at the electrode surface (see the top left inset in Fig. 2). The reduction potential $E^{0'}$ for this system is 0.269 V vs SHE, which closely parallels that for wild-type azurin (WTAZ) immobilized on a decane-1-thiol (DT) SAM , centreed at 0.272 V at pH 7.7 [25]. This likely hints that the orientation of immobilized azurin on MTM and DT monolayers is the same. The $E^{0'}$ for adsorbed HT-Azu is very close, though slightly less positive, to what we obtained for the freely diffusing protein (0.288 V; see Figure S2 in the SI for the corresponding cyclic voltammogram). This finding indicates that the properties of the metal site are scarcely influenced by the immobilization on the SAM, similarly to what was

previously observed for WTAZ adsorbed on different alkanethiolate SAMs [25]. The surface coverage for azurin was estimated to be 1.5 pmol cm^{-2}. This data corresponds to a sub-monolayer coverage, as the full monolayer for azurin on hydrophobic SAMs was estimated to be as high as 25 pmol cm^{-2} [41]. Our value for the surface coverage is in line, although slightly lower, with previously reported values of surface coverage of azurin on alkanethiol-based SAMs on Au, whose values were found to range from 4.2±0.6 pmol cm^{-2} on decanethiol [42] to 7±1 pmol cm^{-2} on octanethiol [41].

The ET kinetics between the immobilized protein and the electrode was investigated by the Laviron method, recording CVs at different scan rates [36]. This method allows for the kinetic constant for ET at zero driving force (k_s) to be determined for strongly adsorbed electrochemical systems. It was previously reported [24, 25] that, in order to obtain k_s for surface-immobilized azurin, one must perform measurements at variable scan rates at pH values falling outside the 6.0-8.5 pH range, where the ET process is coupled to a slower proton transfer associated with (de)protonation of His35. For this reasons, we performed variable scan rate measurements at pH 9.2. Some representative CVs, obtained at increasing scan rates, are shown in Fig 3. For HT-Azu on MTM, we obtained $k_s = 1093 \pm 100$ s^{-1}.

Well defined cathodic and anodic peaks can be obtained by applying scan rates as high as 80 V/s, thus providing evidences for the robustness of the protein/SAM adduct and for its efficiency in terms of ET. The obtained k_s value is higher than that for WTAZ on DT, which was estimated to be 570 s^{-1} at pH 9.2 [25].

The ET process from a SAM-immobilized redox protein to an electrode can be described as a tunneling mechanism through a non homogeneous medium; in the present case, through three different media (the protein matrix, the interface between the protein and the SAM head group, and the SAM), each characterized by its exponential decay factor ($\beta_{protein}$, β_{inter} and β_{SAM}, respectively) [26]. The rate constant for proteins immobilized on SAMs can be then expressed as

follows [26]:

$$k_s = k_0^{'}\, e^{-\beta_{protein} d_{protein}}\, e^{-\beta_{inter} d_{inter}}\, e^{-\beta_{SAM} d_{SAM}} \quad (1)$$

where $d_{protein}$ is the distance between the redox active centre of the biomolecule and the electronic coupling site located on the protein surface at the interface with the SAM; d_{inter} represents the intermolecular distance between the latter electronic coupling site and the one located on the SAM head group; d_{SAM} is the thickness of the SAM.

We can use Eq.1 to gain insights into the features of the MTM monolayer. We can compare the rate constant values that we obtained for HT-Azu on MTM with that for WTAZ on DT: we can safely assume that the orientation of the protein is the same on both SAMs, therefore the differences in k_s are not related to either $e^{-\beta_{protein} d_{protein}}$ nor $e^{-\beta_{inter} d_{inter}}$ terms, and $k_0^{'}$ also takes the same value in both cases. The thickness of the DT SAM can be evaluated to be $13.5 \mathring{A}$ by considering a $1.5 \mathring{A}$ contribution from each methylene group [43, 44], and that of the MTM monolayer was previously estimated by means of spectroscopic ellipsometry, yielding a $18.9 \mathring{A}$ value [31]. We then have the following:

$$570 = const\, e^{-\beta_{DT} 13.5} \quad (2)$$

$$1093 = const\, e^{-\beta_{MTM} 18.9} \quad (3)$$

By dividing Eq.3 by Eq.2, we get $\beta_{MTM} = 0.79 \beta_{DT}$. If we assign the attenuation factor β_{DT} a value of $0.87 \mathring{A}^{-1}$[45], we get $\beta_{MTM} = 0.69\ \mathring{A}^{-1}$, which is consistent with previously reported β for aromatic SAMs [46, 47].

3.2. Vectorial electron transfer

So far, we have described the intermolecular ET process occurring between the protein active site and the electrode. Nevertheless, our engineered azurin also bears a C-terminal hexahistidine tag, which is known to bind metal ions, such as Cu^{2+}. We incubated our functionalized electrodes in a 5 mM aqueous solution of $CuSO_4$. After thoroughly rinsing the electrode to get rid of unbound

Cu^{2+} ions, CVs were recorded. A typical result is shown in Fig.4: both cathodic and anodic signals, corresponding to the faradic process involving the native copper T1 site, are still present, featuring an E^0 value that is almost unaltered with respect to that displayed before incubation with Cu^{2+} solution. Furthermore, a second anodic signal, which lacks its cathodic counterpart, appears at an $E_{p,a}$ value of 0.504 V. While in the CV shown in Fig.2 the cathodic and anodic peaks area are roughly the same, the area of the single cathodic peak in Fig.4 approximately corresponds to the sum of that of the two anodic signals.

The electrochemical features of the CV displayed in Fig.4 are consistent with the following scenario: after incubation with the Cu^{2+} solution, the immobilized HT-Azu molecules bind an additional copper ion, very likely coordinated by the side chains of the C-terminal histidines. Therefore, two metal, redox active centres are now present in each azurin molecule, namely the naturally occurring Cu T1 site (native hereafter) and the exogenous one (exo hereafter), *i.e.* the His-tag-coordinated copper ion. Control experiments support these hypothesis: in fact, further incubation with 10 mM EDTA, pH 7.0 causes disappearance of the exo signal without affecting the native one, which can be restored via further incubation with a Cu^{2+} aqueous solution. Moreover, incubation of surface immobilized WTAZ, which lacks the C-terminal hexahistidine tag, in a 5 mM aqueous solution of $CuSO_4$ yields no additional electrochemical signal to those of the native Cu redox centre (data not shown). The same negative response is obtained when gold electrodes functionalized with MTM only are incubated in a Cu^{2+} aqueous solution. Therefore, the second electrochemical signal in Fig. 4 can be unambiguously ascribed to the exo metal centre.

Experimental evidences of the presence of the additional exo copper ion were provided by KPFM and XPS measurements. The stepwise functionalization protocol, which eventually leads to the presence of surface-immobilized azurin bearing both native and exo centre, consists of three steps, namely i) formation of an MTM-based SAM, ii) HT-Azu adsorption and iii) exo Cu uptake, coordinated by the His-tag. KPFM and XPS are extremely sensitive techniques

in order to characterize the Au surface evolution during each functionalization step. In particular, KPFM measurements provide to monitor the surface potential (a.k.a. contact potential difference, CPD) of the Au surface. Panel A of Fig.5 displays the relative CPD changes during all the steps respect to the potential of the pristine gold substrate (*i.e.* $CP_{Au} = 0$ mV). Hence, the measured CPD corresponds to the changing of the charge density of the overlayer (see ref. [48] and references therein). The 1^{st} step shows a dramatic shift of CPD equal to 300 mV. The protein adsorption (2^{nd} step) results in the solvent exposure of the hydrophilic face of the protein causes a further potential variation (CPD $\approx$ 620 mV). Such a variation can be ascribed to the fact that the hydrophobic -OCH_3 terminal group of the SAM gets involved in the hydrophobic interaction with the azurin, which exposes its hydrophilic face to the solution, as it closely parallels the one that has been observed for a change from hydrophobic to hydrophilic terminal group [35] of an oligoarylene thiol SAM. The 3^{rd} step yields a CPD of about -80 mV, due to the adsorption of the exo copper atom, most likely through coordination by the His-tag.

The presence of Cu atom onto the Au surface has been confirmed by XPS analysis. The presence of the protein film has been verified by monitoring the presence of gold (Au4f), nitrogen (N1s) carbon (C1s), oxygen (O1s), sulphur (S2p) and copper (Cu_{NAT}2p) contributions in the measured spectra (data not shown). Being XPS a surface-sensitive technique, the gold contribution decreases with the increasing of multi-layer thickness. C and O contributions do not change appreciably due to the presence of contaminants and constituents of the adsorbed molecules such as SAM and protein. S contribution is measured in all the samples, except for the bare gold. Finally, N and Cu_{NAT} contributions, due to the presence of the protein, were only measured after the 2^{nd} and 3^{rd} steps. In particular, the measured ratio between these two elements (Cu_{NAT}/N $= 0.007 \pm 0.001$) is in good agreement with literature [49]. It is important to point out that the ratio value does not directly correspond to the stoichiometry of the system because it depends on the position of the atoms inside the sample. In particular, being the copper close to the interface with SAM, its contribu-

tion results to be underestimated. Panel B of Fig.5 reports the XPS spectra acquired before (black line) and after (red line) the 3^{rd} step, in order to gain further evidences of the presence of a protein-bound, exogenous copper ion. X and Y axes represent the binding energy (BE) of the initial bound state of the photoelectron and total counts (CPS), respectively. The first evidence of the immobilization of the exo copper ion on the immobilized SAM/protein layer is provided by the increase of one order of magnitude of the copper peak after the 3^{rd} (red) with respect to the black one. The measured copper signal depicted is contributed by both Cu_{NAT} and Cu_{EXO}. We estimated the relative amount of the two different copper atoms by using a simple geometrical model which takes into account both the effects of a) the photoelectron mean free path λ and b) the different position of the two ions within the protein. λ defines the effective sub-surface region probed by the XPS technique corresponding to about 1 nm, while for b), we considered all the Cu_{EXO} atoms as lying on the surface (depth = 0 nm) and all the Cu_{NAT} ones at a depth of about 2 nm [49]. Under this approximation, the ratio between the areas A of the Cu peaks measured after and before the 3^{rd} step step can written in terms of number of atoms of the probed region $N_{Cu_{NAT}}$ and $N_{Cu_{EXO}}$ as in the following relationship:[50]

$$\frac{A_{3^{rd}step}}{A_{2^{nd}step}} = \frac{\alpha_l N_{Cu_{EXO}} + \beta_l N_{Cu_{NAT}}}{\beta_l N_{Cu_{NAT}}}, \quad \alpha_l = exp\{-z/\lambda\}|_{z=0}\, \beta_l = exp\{-z/\lambda\}|_{z=2} \tag{4}$$

The ratio can be measured directly from the spectra, and the obtained value is 8.4 ± 0.4, while α_l and β_l represent the penetration length for atoms at the surface (z = 0) and buried (z = 2), respectively. The solution of eq.4 yields $N_{Cu_{NAT}} \approx N_{Cu_{EXO}}$, suggesting that after the 3^{rd} step each protein molecule contains approximately two copper ions. A further issue regards the energy position and the shape of the peak, which do not show an appreciable difference between the two steps: this finding indicates that for both and Cu_{NAT} and Cu_{EXO} the copper ion is coordinated, and that the overall electron donating effect of the two coordinative kernels is similar.

No significant changes in the CV could be detected upon continued cycling, indicating that the copper ions in the exo sites are stable even upon repeated reduction/oxidation cycles, which most likely do not proceed through a Cu^0 metallic state. Most notably, the fact that the electrochemical signals displayed in Fig.4 are conserved after the first cycle implies that, although the cathodic counterpart of the faradic process at the exo site is lacking, there must be a mechanism which can restore its Cu^{2+} state.

Such electrochemical features very closely parallel those observed for surface immobilized diheme *P. stutzeri* cytochrome c_4 [11], *P. haloplanktis* cytochrome c_4 [13] and diheme *S. baltica* cytochrome c [12], where vectorial electron transfer processes took place. These proteins possess two separate heme centres, whose electron exchange mechanism to/from the electrode was proven to be mediated by their relative position with respect to the surface: in particular, the ET processes from the distal heme is mediated by the vicinal one, lying closer to the surface. This leads to an unsymmetrical electrochemical behavior [11, 13, 12], composed by a *single two-electrons* peak in one scanning direction and in *two one-electron peaks* when scanning the potential in the opposite direction. If the vicinal heme has a higher (more positive) $E^{0'}$ than the distal heme, two one-electron cathodic peaks would be observed, and a single $2e^-$ anodic signal would be recorded. Reverse electrochemical features would be obtained if the vicinal heme featured a more negative $E^{0'}$ than the distal one. The striking resemblance of the electrochemical response of the system under investigation with that of adsorbed diheme cytochromes suggests that vectorial electron transfer processes between exo and native metal sites and the Au electrode can be invoked.

The behavior of the system under investigation can be framed into the following rationale (see Fig.6): two redox active sites are present, native and exo (Cu_{NAT} and Cu_{EXO}, respectively), and the difference between their reduction potentials is large enough to allow the detection of separate electrochemical signals. The native site has a lower $E^{0'}$, and is located much closer to the surface than the exo site, which features a significantly higher reduction potential. Starting from an anodic poise, both centres are in their oxidized state, Cu^{2+}_{NAT}

and Cu^{2+}_{EXO}. When performing a cathodic scan, thermodynamically the first centre to undergo reduction should be the exo one, but it cannot communicate directly with the electrode, as it lies too far away from it. Therefore, no cathodic peak for exo can be observed until the potential of the more negative native site is reached. Only when the native centre is reduced electrons can flow from the electrode to the native Cu and can also be immediately transferred to exo, through a thermodynamically favored, fast intramolecular ET. Both native and exo centres are reduced, originating the fast two-ET process associated with the $2e^-$ cathodic signal in Fig.4 and yielding the doubly reduced state, Cu^{1+}_{NAT} and Cu^{1+}_{EXO}. During the anodic scan instead, the two centres are sequentially oxidized: the native centre is the first one to undergo oxidation, generating a mixed oxidized-reduced state $Cu^{2+}_{NAT}/Cu^{1+}_{EXO}$, while the exo copper ion is oxidized at more positive potential, and its ET to the electrode takes place via the native Cu.

The changes in the electrochemical behavior of the present system as a function of the scan rate are also worth mentioning (see Fig. 7): in fact, the anodic signal associated with the exo Cu centre cannot be observed anymore for scan rates higher than 1 Vs^{-1}. This finding indicates that the value of the rate constants for the intermolecular ET (between native Cu centre and the electrode) and for the intramolecular ET (between exo and native copper ions) significantly affects the electrochemical response of the system.

In order to gain further insights on the rate of the intramolecular ET process, we adapted a previously published model for intramolecular ET in metalloproteins featuring two metal centres [51, 11]. In the model depicted in Panel A of Fig.8, C_1 and C_2 represent the native and exogenous copper centres of HT-Azu, respectively.

The surface concentration of reduced C_1, labelled as $C_1^{red,surf}$, can be expressed as:

$$C_1^{red,surf} = P_1\Gamma \tag{5}$$

where Γ is the total surface concentration of the protein HT-Azu and P_1 is the

fraction of the reduced species C_1, with $P_1 \leq 1$.

It follows that surface concentration of oxidized C_1, $C_1^{ox,surf}$, can be expressed as:

$$C_1^{ox,surf} = (1 - P_1)\Gamma \tag{6}$$

Similarly, we can define $C_2^{red,surf}$ and $C_2^{ox,surf}$ as:

$$C_2^{red,surf} = P_2\Gamma \tag{7}$$

and

$$C_2^{ox,surf} = (1 - P_2)\Gamma \tag{8}$$

Clearly, $P_2 \leq 1$. Under the assumption of α=0.5, the rate constant for the ET processes between C_1 and the electrode can be expressed as follows:

$$k_1(t) = k_0\, e^{-\frac{FE(t)}{2RT}} \tag{9}$$

$$k_2(t) = k_0\, e^{\frac{FE(t)}{2RT}} \tag{10}$$

where k_0 is the k_{ET} for E = E^0 and

$$E(t) = E_i + vt \tag{11}$$

with E_i the starting potential of the voltammetric scan and v is the scan rate.

The current I that goes through the interface between the electrode and the C_1 centre can be described by the following expression:

$$I = A\Gamma F k_0\{e^{-\frac{FE(t)}{2RT}}(1 - P_1) - e^{\frac{FE(t)}{2RT}} P_1\} \tag{12}$$

But P_1, and obviously also $(1 - P_1)$, also depend on the intramolecular electron exchange process taking place between C_1 and C_2, which can be described in terms of rate constants k_3 and k_4. Please note that k_3 and k_4 are not dependent on the electrode potential, and therefore are true rate constants, as they do

not depend on time variation of the potential during the CV scan, at variance with $k_1(t)$ and $k_2(t)$ [51].

The time-dependent variation of the P_1 and P_2 values are related by the following differential equation system:

$$\frac{dP_1}{dt} = k_1(t)(1-P_1) - k_2(t)P_1 - k_3P_1(1-P_2) + k_4(1-P_1)P_2 \quad (13)$$

$$\frac{dP_2}{dt} = k_3P_1(1-P_2) - k_4(1-P_1)P_2 \quad (14)$$

This differential equation system cannot be solved analytically, but can be resolved by numerical approaches such as the Runge-Kutta method, by inserting values for k_s, k_3, k_4, E_i and v. The numerical approach to the solution of the system was implemented on Matlab. Solving the differential equation system yields the time dependance of P_1 and P_2. The former can be then inserted in eq.12. The aforementioned approach was used to simulate the electrochemical response displayed in Fig.4, in order to calculate the rate constants k_3, k_4, assuming for k_s a value of 1000 s^{-1}. The best accordance with the experimental data in Fig.4 was found for 1800 s^{-1} for k_3 and 0.1 s-1 for k_4, at a scan rate of v=50 mv s^{-1}. The simulated CV is displayed in Panel B of Fig.8. Values of rate constants for long range, intramolecular electron transfer in azurin from *Pseudomonas aeruginosa* have been previously reported [52, 53, 54]: such values display a marked dependence on the pH, as they can range from 285 s^{-1} at pH 4 to 15 s^{-1} at slightly alkaline pH values. These values are invariably smaller than that obtained in the present study, but the differences can be tentatively ascribed to different electron transfer pathways being involved in the intramolecular ET processes: in fact, the aforementioned values were obtained by pulse radiolysis generating a $RSSR^-$ anion at the disulfide cystine formed by residues 3 and 27, while in the present case the second centre is probably located at a different position on the protein surface, though probably at comparable distance. The three-dimensional structure of HT-Azu is not presently available to support this hypothesis, but the significant effect of the composition of the protein matrix separating donor and acceptor on the rate of ET processes has been widely

investigated [55, 56].

4. Conclusions

We presented a bio-(in)organic interface which could serve as a model system to investigate the molecular determinants of biological vectorial electron transfer. Among the most important features of our approach are its versatility and simplicity: the use of C- or N-terminal His-tag is now possible on almost any system; therefore, the same strategy can be applied to introduce a novel, exogenous redox centre in virtually any protein. The use of MTM monolayers in the design of such interfaces can also be extended to robustly immobilize any protein with a sufficiently large, surface exposed hydrophobic patch. Nevertheless, what is characteristic to this system, and crucial to its electrochemical features, is the spatial position of the two metal centres with respect to the surface, which causes the intra- and intermolecular ET rate constants to differ largely enough, to be able to turn off the former process, by adjusting the scan rates.

5. Acknowledgements

This work was supported by a grant from the Ministero dell'Universit e della Ricerca (MIUR) of Italy (Programmi di Ricerca Scientifica di Rilevante Interesse Nazionale 2009 prot. n. 20098Z4M5E_002 (MB)). This work was funded by the European Union 7^{th} Framework Programme [FP7/2007?2013] under Grant Agreement No. 280772, Implantable Organic Nanoelectronics (iONE-FP7) project. The authors thank Dr. Derek Jones for enlightening discussions and for the support for the XPS measurements and Dott. Ing. Roberto Borsari and Dott. Ing. Marco Poppi for help with the implementation of the Runge Kutta method for solving the differential equation system.

References

[1] H. B. Gray, J. R. Winkler, Electron tunneling through proteins, Q. Rev. Biophys. 36 (2003) 341–372.

[2] A. J. Gates, S. J. Marritt, J. M. Bradley, L. Shi, D. G. G. McMillan, L. J. C. Jeuken, D. J. Richardson, J. N. Butt, Electrode assemblies composed of redox cascades from microbial respiratory electron transfer chains., Biochem. Soc. Trans. 41 (5) (2013) 1249–53.

[3] C. M. Paquete, R. O. Louro, Unveiling the details of electron transfer in multicenter redox proteins, Acc. Chem. Res. 47 (2014) 56–65.

[4] K. D. Bewley, K. E. Ellis, S. J. Firer-Sherwood, Mackenzie A a nd Elliott, Multi-heme proteins: nature's electronic multi-purpose tool, Biochim. Biophys. Acta 1827 (2013) 938–48.

[5] S. Sharma, G. Cavallaro, A. Rosato, A systematic investigation of multiheme c-type cytochromes in prokaryotes, J. Biol. Inorg. Chem. 15 (2010) 559–571.

[6] I. Daidone, L. Paltrinieri, A. Amadei, G. Battistuzzi, M. Sola, M. Borsari, C. A. Bortolotti, Unambiguous assignment of reduction potentials in diheme cytochromes., J. Phys. Chem. B 118 (2014) 7554–7560.

[7] D. Lovley, Long-range electron transport to Fe (III) oxide via pili with metallic-like conductivity, Biochem. Soc. Trans. 40 (2012) 1186–1190.

[8] N. Polizzi, S. Skourtis, D. Beratan, Physical constraints on charge transport through bacterial nanowires, Faraday Discuss. 155 (2012) 43–61.

[9] N. S. Malvankar, D. R. Lovley, Microbial nanowires: A new paradigm for biological electron transfer and bioelectronics, Chemsuschem 5 (2012) 1039–1046.

[10] L. Morgado, A. P. Fernandes, J. M. Dantas, M. A. Silva, C. A. Salgueiro, On the road to improve the bioremediation and electricity-harvesting skills

of *geobacter sulfurreducens*: Functional and structural characterization of multihaem cytochromes, Biochem. Soc. T. 40 (2012) 1295–1301.

[11] Q. Chi, J. Zhang, T. Arslan, L. Borg, G. W. Pedersen, H. E. M. Christensen, R. R. Nazmudtinov, J. Ulstrup, Approach to interfacial and intramolecular electron transfer of the diheme protein cytochrome c 4 assembled on Au (111) surfaces, J. Phys. Chem.B 114 (2010) 5617–5624.

[12] G. Di Rocco, G. Battistuzzi, C. A. Bortolotti, M. Borsari, E. Ferrari, S. Monari, M. Sola, Cloning, expression, and physicochemical characterization of a new diheme cytochrome c from shewanella baltica os155., J. Biol. Inorg. Chem. 16 (2011) 461–471.

[13] S. Monari, G. Battistuzzi, M. Borsari, G. Di Rocco, L. Martini, A. Ranieri, M. Sola, Heterogeneous Electron Transfer of a Two-Centered Heme Protein: Redox and Electrocatalytic Properties of Surface-Immobilized Cytochrome *c*4, J. Phys. Chem. B 113 (2009) 13645–13653.

[14] W. J. Maalcke, A. Dietl, S. J. Marritt, J. N. Butt, M. S. M. Jetten, J. T. Keltjens, T. R. M. Barends, B. Kartal, Structural basis of biological no generation by octaheme oxidoreductases, J. Biol. Chem. 289 (2014) 1228–1242.

[15] R. Doyle, S. Marritt, J. Gwyer, T. Lowe, M. Cheesman, J. Butt, T. Tikhonova, V. Popov, Contrasting catalytic profiles of multiheme nitrite reductases containing cxxck heme-binding motifs, J. Biol. Inorg. Chem. 18 (2013) 655–667.

[16] P. O. Quintas, A. P. Cepeda, N. Borges, T. Catarino, D. L. Turner, Relative importance of driving force and electrostatic interactions in the reduction of multihaem cytochromes by small molecules., Biochim. Biophys. Acta 1827 (2013) 745–750.

[17] J. Hainfeld, W. Liu, C. Halsey, P. Freimuth, R. Powell, NiNTAgold clusters target his-tagged proteins, J. Struct. Biol. 127 (2) (1999) 185–198.

[18] G. Agarwal, R. Naik, M. Stone, Immobilization of histidine-tagged proteins on nickel by electrochemical dip pen nanolithography, J. Am. Chem. Soc. 125 (24) (2003) 7408–7412.

[19] A. Alessandrini, C. A. Bortolotti, G. Bertoni, A. Vezzoli, P. Facci, Ultra-flat nickel substrates for scanning probe microscopy of polyhistidine-tagged proteins, J. Phys. Chem. C 112 (2008) 3747–3750.

[20] Z. Yang, Y.-P. Zhao, Adsorption of his-tagged peptide to Ni, Cu and Au (100) surfaces: Molecular dynamics simulation, Eng. Anal. Bound. Elem. 31 (2007) 402–409.

[21] G. Bachand, C. Montemagno, Constructing organic/inorganic NEMS devices powered by biomolecular motors, Biomed. Microdevices 2:3 (2000) 402–409.

[22] G. Sigal, C. Bamdad, A. Barberis, J. Strominger, G. Whitesides, A self-assembled monolayer for the binding and study of histidine-tagged proteins by surface plasmon resonance, Anal. Chem. 68 (1996) 490–497.

[23] M. Cascella, A. Magistrato, I. Tavernelli, P. Carloni, U. Rothlisberger, Role of protein frame and solvent for the redox properties of azurin from *Pseudomonas aeruginosa*, Proc. Natl. Acad. Sci. USA 103 (2006) 19641–19646.

[24] L. Jeuken, L. Wisson, F. Armstrong, The kinetics of a weakly electron-coupled proton transfer in azurin, Inorg. Chim. Acta 331 (2002) 216–223.

[25] S. Monari, G. Battistuzzi, C. Dennison, M. Borsari, A. Ranieri, M. J. Siwek, M. Sola, Factors affecting the electron transfer properties of an immobilized cupredoxin, J. Phys. Chem. C 114 (2010) 22322–22329.

[26] K. Fujita, N. Nakamura, H. Ohno, B. S. Leigh, K. Niki, H. B. Gray, J. H. Richards, Mimicking protein - protein electron transfer : Voltammetry of pseudomonas aeruginosa azurin and the thermus thermophilus cu a domain

at ω -derivatized self-assembled monolayers gold electrodes., J. Am. Chem. Soc. 126 (4) (2004) 13954–13961.

[27] S. Monari, G. Battistuzzi, C. A. Bortolotti, S. h. Yanagisawa, K. Sato, C. Li, I. Salard, D. Kostrz, M. Borsari, A. Ranieri, C. Dennison, M. Sola, Understanding the mechanism of short-range electron transfer using an immobilized cupred oxin., J. Am. Chem. Soc. 134 (2012) 11848–51.

[28] D. E. Khoshtariya, T. D. Dolidze, M. Shushanyan, K. L. Davis, D. H. Waldeck, R. van Eldik, Fundamental signatures of short- and long-range electron transfer for the blue copper protein azurin at Au/SAM junctions, Proc. Natl. Acad. Sci. USA 107 (2010) 2757–2762.

[29] N. M. Marshall, D. K. Garner, T. D. Wilson, Y.-G. Gao, H. Robinson, M. J. N ilges, Y. Lu, Rationally tuning the reduction potential of a single cupredoxin beyond the natural range., Nature 462 (2009) 113–116.

[30] A. Operamolla, O. Hassan Omar, F. Babudri, G. Farinola, F. Naso, Synthesis of s-acetyl oligoarylenedithiols via Suzuki-Miyaura cross-coupling, J. Org. Chem. 72 (2007) 10272–10275.

[31] G. Bruno, F. Babudri, A. Operamolla, G. V. Bianco, M. Losurdo, M. M. Giangregorio, O. Hassan Omar, F. Mavelli, G. M. Farinola, P. Capezzuto, F. Naso, Tailoring density and optical and thermal behavior of gold surfaces and nanoparticles exploiting aromatic dithiols., Langmuir 26 (2010) 8430–40.

[32] S. Casalini, G. Battistuzzi, M. Borsari, C. A. Bortolotti, G. Di Rocco, A. Ranieri, M. Sola, Electron transfer properties and hydrogen peroxide electrocatalysis of cytochrome c variants at positions 67 and 80., J. Phys. Chem. B 114 (2010) 1698–706.

[33] S. Casalini, F. Leonardi, C. A. Bortolotti, A. Operamolla, O. H. Omar, L. Paltrinieri, C. Albonetti, G. M. Farinola, F. Biscarini, Mono/bidentate

thiol oligoarylene-based self-assembled monolayers (SAMs) for interface engineering, J. Mater. Chem. 22 (2012) 12155–12163.

[34] S. Casalini, M. Berto, F. Leonardi, A. Operamolla, C. A. Bortolotti, M. Borsari, W. Sun, R. Di Felice, S. Corni, C. Albonetti, O. H. Omar, G. M. Farinola, F. Biscarini, Self-assembly of mono- and bidentate oligoarylene thiols onto polycrystalline Au, Langmuir 29 (2013) 13198–13208.

[35] S. Casalini, M. Berto, C. Bortolotti, G. Foschi, M. Di Lauro, H. Omar, A. Liscio, L. Pasquali, M. Montecchi, G. Farinola, M. Borsari, Electrowetting of nitro-functionalized oligoarylene thiols self-assembled on polycrystalline gold, ACS Appl. Mat. Inter. 7 (2015) 3902–3909.

[36] E. Laviron, General expression of the linear potential sweep voltammogram in the case of diffusionless electrochemical systems., J. Electroanal. Chem. 101 (1979) 19–28.

[37] H. Nar, A. Messerschmidt, R. Huber, M. van de Kamp, G. Canters, Crystal structure analysis of oxidized *Pseudomonas aeruginosa* azurin at ph 5.5 and ph 9.0. a ph-induced conformational transition involves a peptide bond flip., J. Mol. Biol. 221 (1991) 765–772.

[38] T. V. Pyrkov, A. O. Chugunov, N. a. Krylov, D. E. Nolde, R. G. Efremov, PLATINUM: a web tool for analysis of hydrophobic/hydrophilic organization of biomolecular complexes., Bioinformatics 25 (2009) 1201–2.

[39] R. G. Efremov, A. O. Chugunov, T. V. Pyrkov, J. P. Priestle, A. S. Arseniev, E. Jacoby, Molecular Lipophilicity in Protein Modeling and Drug Design, Curr. Med. Chem. 14 (2007) 393–415.

[40] L. Paltrinieri, M. Borsari, G. Battistuzzi, M. Sola, C. Dennison, B. L. de Groot, S. Corni, C. A. Bortolotti, How the dynamics of the metal-binding loop region controls the acid transition in cupredoxins., Biochemistry 52 (2013) 7397–7404.

[41] B. Fleming, S. Praporski, A. Bond, L. Martin, Electrochemical quartz crystal microbalance study of azurinelectrochemical quartz crystal microbalance study of azurin, Langmuir 24 (2008) 323–327.

[42] Q. Chi, J. Zhang, J. Andersen, J. Ulstrup, Ordered assembly and controlled electron transfer of the blue copper protein azurin at gold (111) single-crystal substrates, J. Phys. Chem. B 105 (2001) 4669–4679.

[43] C. Bain, E. Troughton, T. Yu-Tai, J. Evall, G. M. Whitesides, R. G. Nuzzo, Formation of monolayer films by the spontaneous assembly of organic thiols from solution onto gold, J. Am. Chem. Soc. 111 (1989) 321–335.

[44] P. E. Laibinis, C. D. Bain, R. G. Nuzzo, G. M. Whitesides, Structure and wetting properties of ω-alkoxy-n-alkanethiolate monolayers on gold and silver, J. Phys. Chem. 99 (1995) 7663–7676.

[45] R. E. Holmlin, R. Haag, M. L. Chabinyc, R. F. Ismagilov, A. E. Cohen, A. Terfort, M. A. Rampi, G. M. Whitesides, Electron transport through thin organic films in metal - insulator - metal junctions based on self-assembled monolayers, J. Am. Chem. Soc. 123 (2001) 5075–5085.

[46] F.-r. F. Fan, J. Yang, L. Cai, D. W. Price, S. M. Dirk, D. V. Kosynkin, Y. Yao, A. M. Rawlett, J. M. Tour, A. J. Bard, Charge transport through self-assembled monolayers of compounds of interest in molecular electronics, J. Am. Chem. Soc. 19 (2002) 5550–5560.

[47] B. Kim, J. M. Beebe, Y. Jun, X. Zhu, C. D. Frisbie, Correlation between homo alignment and contact resistance in molecular junctions : Aromatic thiols versus aromatic isocyanides, J. Am. Chem. Soc. 128 (2006) 4970–4971.

[48] A. Liscio, V. Palermo, P. Samorí, Nanoscale quantitative measurement of the potential of charged nanostructures by electrostatic and kelvin probe force microscopy: Unraveling electronic processes in complex materials, Acc. Chem. Res. 43 (2010) 541–550.

[49] A. Alessandrini, M. Gerunda, P. Facci, B. Schnyder, R. Kotz, Tuning molecular orientation in protein films, Surf. Sci. 542 (2003) 64–71.

[50] F. Himpsel, F. McFeely, A. Taleb-Ibrahimi, J. Yarmoff, G. Hollinger, Microscopic structure of the sio_2/si interface, Phys. Rev. B 38 (1988) 6084–6096.

[51] A. Welinder, J. Zhang, A. Hansen, K. Moth-Poulsen, H. Christensen, A. Kuznetsov, T. Bjornholm, J. Ulstrup, Voltammetry and electrocatalysis of achromobacter xylosoxidans copper nitrite reductase on functionalized au(111)-electrode surfaces, Z. Phys. Chem. 221 (2007) 1343–1378.

[52] O. Farver, I. Pecht, Long range intramolecular electron transfer in azurins, J. Am. Chem. Soc. 43 (2010) 541–550.

[53] O. Farver, N. Bonander, L. Skov, I. Pecht, The ph dependence of long range electron transfer in azurins, Inorg. Chim. Acta 24 (1996) 127–133.

[54] O. Farver, L. Jeuken, G. Cnters, I. Pecht, Role of ligand substitution on long-range electron transfer in azurins, Eur. J. Biochem. 267 (2000) 3123–3129.

[55] J. Winkler, H. Gray, Electron tunneling in proteins: role of the intervening medium, J. Biol. Inorg. Chem. (1997) 399–404.

[56] J. Winkler, Electron tunneling pathways in proteins, Curr. Opin. Chem. Biol. 4 (2000) 192–198.

Figures

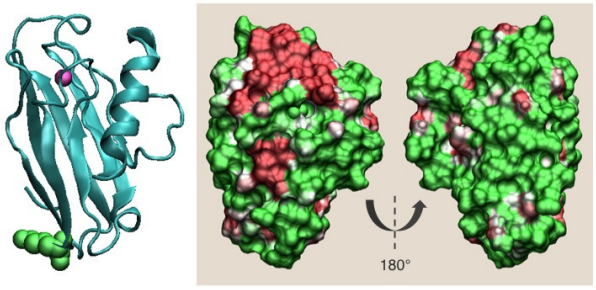

Figure 1: Left: Cartoon representation of the backbone of wild-type azurin. The Cu atom is represented as a pink sphere, and the C-terminal residue (Lys128) in green Van der Waals spheres. Centre and Right: Surface Hydrophobic Potential of wild type azurin from *P. aeruginosa*, calculated with the Platinum web server. Hydrophobic regions and hydrophilic regions are depicted in red and green, respectively.

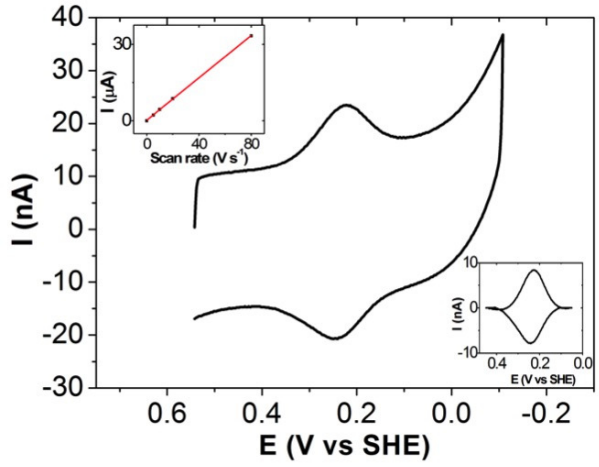

Figure 2: Cyclic voltammogram for HT-Azu immobilized on a polycrystalline Au electrode functionalized with MTM self-assembled monolayer. Working solution: 10 mM Hepes, 0.1M KCl, pH 7.3. Scan rate 50 mV/s. Top left inset: plot of the scan rate dependance of the cathodic peak current. Bottom left inset: electrochemical signal after subtraction of the background current, which corresponds to the current recorded for the polycrystalline Au electrode functionalized with MTM self-assembled monolayer before incubation with HT-Azu.

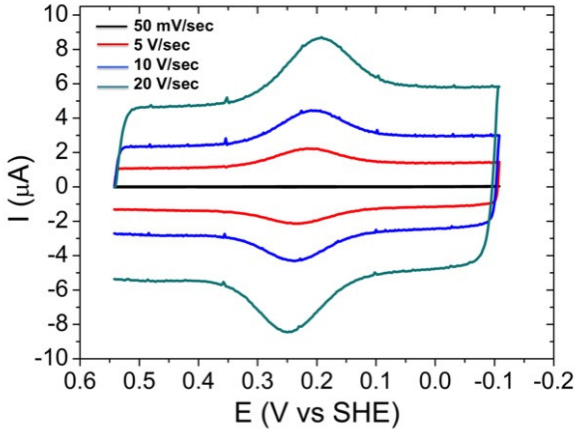

Figure 3: Scan rate dependance of the CVs obtained for HT-Azu immobilized on a MTM SAM on polycrystalline Au electrodes.

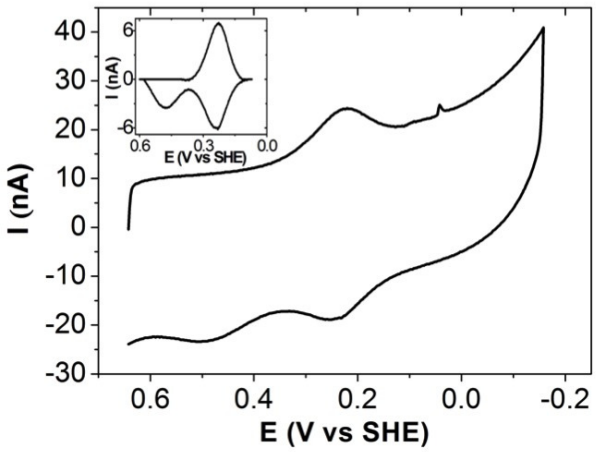

Figure 4: Cyclic voltammogram for HT-Azu immobilized on a polycrystalline Au electrode functionalized with MTM self-assembled monolayer, after incubation with a 5 mM aqueous solution of $CuSO_4$. Working solution: 10 mM Hepes, 0.1M KCl, pH 7.3. Scan rate 50 mV/s.

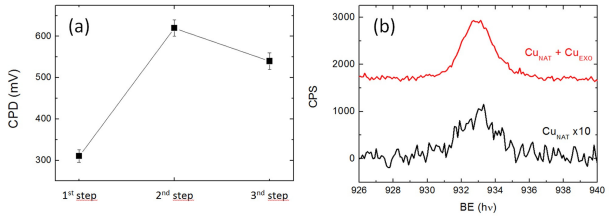

Figure 5: Panel A: CPD, obtained by means of KPFM measurements, at each functionalization step is shown. The black broken line is only a guide for the eye. Panel B: Overlay of the two XPS spectra corresponding to the Cu peak, black for the HT-Azu adsorption and red for the exo Cu uptake.

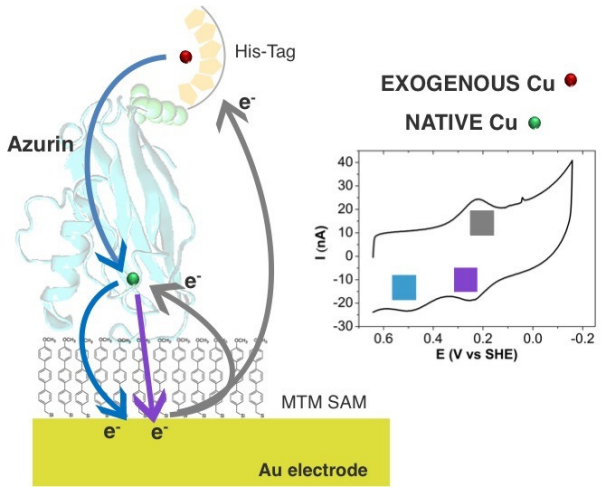

Figure 6: Schematic representation of the ET processes underlying the electrochemical features in Fig.4, displayed in the box on the upper right corner. The single two-electrons cathodic peak, labelled with a grey box, is associated with the simultaneous reduction of both centres. The anodic signal lying at $\approx E_{p,a} = +0.25$ V (purple label) derives from the intermolecular one-electron ET from native Cu to the electrode, while the second anodic signal (tan colored) comes from the one-electron oxidation of the exo Cu, whose ET to the electrode takes place via the native Cu.

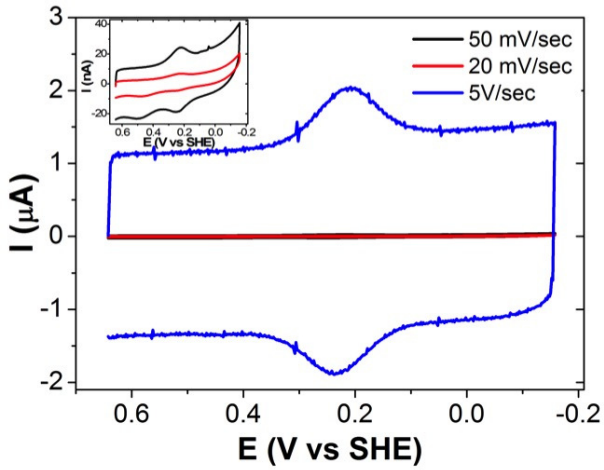

Figure 7: Cyclic voltammograms at different scan rates for HT-Azu immobilized on a polycrystalline Au electrode functionalized with MTM self-assembled monolayer, after incubation with a 5 mM aqueous solution of $CuSO_4$. Working solution: 10 mM Hepes, 0.1M KCl, pH 7.3. In the inset, only the voltammograms recorded at low scan rates (20 mV/s and 50 mV/s, in red and black, respectively, are depicted, as their details cannot be appreciated in the full picture.

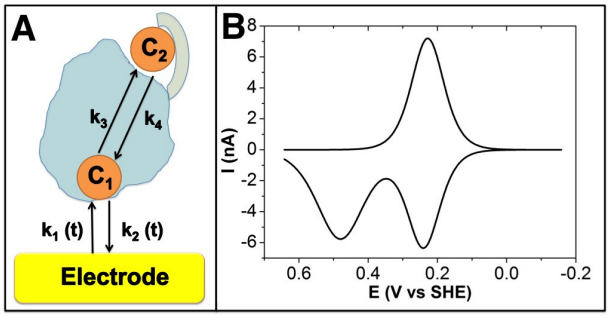

Figure 8: Panel A: Scheme of the inter- and intramolecular ET processes for immobilized HT-Azu with exo copper centre, as discussed in the model adapted from refs. [51] and [11], which was used to calculate the intramolecular rate constants k_3 and k_4. Panel B: Simulated cyclic voltammogram for HT-Azu with exo copper centre adsorbed on an MTM SAM on gold electrodes.